

Measurement Induced Magic Resources

Gong-Chu Li,^{1,2,3,4} Lei Chen,^{1,2,3,4} Si-Qi Zhang,^{1,2,3,4} Xu-Song Hong,^{1,2,3,4}
Huaqing Xu,^{1,2,3,4} Yuancheng Liu,^{1,2,3,4} You Zhou,^{5,4,*} Geng Chen,^{1,2,3,4,†}
Chuan-Feng Li,^{1,2,3,4,‡} Guang-Can Guo,^{1,2,3,4} and Alioscia Hamma^{6,7,8,§}

¹*CAS Key Laboratory of Quantum Information, University of Science and Technology of China, Hefei, Anhui 230026, China.*

²*Anhui Province Key Laboratory of Quantum Network, Hefei, Anhui 230026, China.*

³*CAS Center For Excellence in Quantum Information and Quantum Physics,
University of Science and Technology of China, Hefei, Anhui 230026, China.*

⁴*Hefei National Laboratory, Hefei 230088, China*

⁵*Key Laboratory for Information Science of Electromagnetic Waves
(Ministry of Education), Fudan University, Shanghai 200433, China*

⁶*Dipartimento di Fisica ‘Ettore Pancini’, Università degli Studi di Napoli Federico II, Via Cintia 80126, Napoli, Italy*

⁷*INFN, Sezione di Napoli, Italy*

⁸*Scuola Superiore Meridionale, Largo S. Marcellino 10, 80138 Napoli, Italy*

Magic states and magic gates are crucial for achieving universal quantum computation, but important questions about how magic resources should be implemented to attain maximal quantum advantage have remained unexplored, especially in the context of measurement-based quantum computation (MQC). This work bridges the gap between MQC and the resource theory of magic by introducing the key concepts of “invested” and “potential” magic resources. The former quantifies the magic cost associated with MQC, serving as both a resource witness and a feasible upper bound for the practical realization, and is gate-order independent; The latter represents the maximal achievable magic resource in a given graph structure defining MQC. We utilize both concepts to analyze quantum Fourier transform (QFT) and provide a fresh perspective on the universality of MQC, highlighting the crucial role of non-Pauli measurements in injecting magic. In particular, we theoretically prove that high-dimensional graphs can generate an exponential advantage of MQC compared to classical computing. We demonstrate experimentally our theoretical findings in a high-fidelity four-photon setup, surpassing conventional magic state injection (MSI) methods in both qubit efficiency and resource utilization. Our findings pave the way for future research exploring magic resource optimization and novel distillation schemes within the MQC framework, advancing fault-tolerant universal quantum computation.

Introduction — The ultimate goal of quantum computation is to realize large-scale, fault-tolerant, universal quantum computation [1]. To this end, quantum error correction codes are used to encode logical qubits and introduce sets of fault-tolerant universal gates [2–4]. Within such a framework, T states/gates, often referred to as magic states/gates [5], have been recognized as crucial resources, which can be quantified by the corresponding resource theory [6–8].

Magic resources connect closely with magic distillation [4, 5, 9], magic synthesis [10–12] tasks, and classical simulation complexity [13–15]. At the core of these discussions is the celebrated Gottesman-Knill theorem [13–15], which moves beyond the first layer of computation, i.e., injecting k magic states to Clifford circuits exponentially increases the complexity of classical simulation as $2^{O(k)} \text{poly}(n)$ of an n -qubit system. From such a perspective, universal quantum computation is characterized by an exponential increase in resource requirements for classical computation, quantified by the magic resource present.

A reliable measure of magic resource should satisfy three key properties: faithfulness (zero for Clifford gates and stabilizer states), non-increasingness under free operations (i.e., Clifford operations), and (sub-)additivity

(for independent components). These ensure the consistency and practicality of the measure in real quantum computations. While measures like mana [16], robustness [11], thauma [17], and nullity [18] satisfy faithfulness and Clifford invariance, they lack the additivity property. Recent approaches based on stabilizer norm [11], stabilizer Rényi entropy [7, 8], and Gottesman-Kitaev-Preskill codes [19] have successfully addressed this limitation, providing measures that fulfill all three desired criteria.

Recently, the issue of the magic resource cost of non-Pauli measurements has risen to attention [20, 21]. However, a significant gap remains in our understanding of their fundamental role within the framework of measurement-based quantum computation (MQC) [22]. MQC, a prominent paradigm in quantum computing, relies on the preparation of cluster states, which are stabilizer states associated with a graph and thus inherently lack magic resources. Universality in MQC is achieved through consecutive non-Pauli single-qubit measurements on these graph stabilizer states. This highlights a crucial insight that non-Pauli measurements are responsible for generating magic resources, whereas the source of MQC’s universality has traditionally been attributed to the rich entanglement structure of graph states [23, 24].



FIG. 1. Cartoon showing the relationship between invested magic resources (\mathcal{M}), potential magic resources (\mathcal{P}), and reserved magic resources (\mathcal{R}) using a water-pouring analogy.

While magic resource distillation/synthesis is a well-established approach for achieving universal quantum computation, the role of non-Pauli measurements has been less explored, and their critical role in achieving quantum advantage is not well understood. The current work introduces two new measures for magic resources—*invested* and *potential*—that address the gap in current quantum resource theories, shedding light on how measurement-based processes contribute to achieving quantum advantage, particularly in the context of MQC where non-Pauli measurements play a crucial role.

This work consists of two parts: Theory and Experiment. In the first part, we establish the theory of *invested magic resources* (\mathcal{M}) and *potential magic resources* (\mathcal{P}) as sketched in Fig. 1, and will be addressed later. In the second part, we experimentally demonstrate the effectiveness of injecting magic resources through MQC in a four-photon experiment, involving a single-qubit rotation and Quantum Fourier Transform (QFT) tasks. We show that non-Pauli measurements, combined with the entanglement structure of graph states, are essential for the universality of MQC. Our framework provides a novel way of quantifying the magic resources needed for these measurements, thereby advancing our understanding of MQC’s computational power.

Review of MQC — The setup of MQC starts with a graph state $|G\rangle$, which is an entangled state of n qubits defined by a graph $G = (V, E)$ with n vertices at $|+\rangle = (|0\rangle + |1\rangle)/\sqrt{2}$ and edges representing controlled-Z (CZ) gates. Graph states are a special type of stabilizer state, meaning they possess a set of stabilizing operators that leave the state unchanged. MQC relies on preparing a suitable graph state and performing a series of adaptive single-qubit measurements in the X-Y plane of the Bloch sphere. The final state of the computation is locally Pauli equivalent to the desired target state. Based on the stochastic outcomes of the measure-

ments and additional Pauli corrections, MQC becomes a universal quantum computation platform. This process can be summarized as the CME pattern [25, 26], consisting of Entanglement (preparing the graph state), Measurement (adaptive single-qubit measurements), and Correction (Pauli corrections).

CME relies on the fact that any unitary operation can be decomposed into a sequence of CZ gates and J gates, $J(\theta) = \frac{1}{\sqrt{2}} \begin{pmatrix} 1 & e^{i\theta} \\ 1 & -e^{i\theta} \end{pmatrix}$. This decomposition process is known as J-decomposition. Each J gate in the decomposition corresponds to a small CME structure. For example, $J(\theta)$ on the qubit 2 can be implemented as $J(\theta) := X_2^{s_1} M_1^{-\theta} E_{12}$, where E_{12} represents a CZ gate between qubits 1 and 2, $M_1^{-\theta}$ denotes a measurement on the first qubit in the basis $(|0\rangle \pm e^{-i\theta}|1\rangle)/\sqrt{2}$, s_1 is the signal of measurement outcome, and $X_2^{s_1}$ is a Pauli X correction applied to the second qubit based on s_1 . This equation illustrates how the action of $J(\theta)$ on a state $|\psi\rangle$ can be achieved using an auxiliary qubit, i.e., the second qubit, initialized in the $|+\rangle$ state and an appropriate MQC procedure. For more complex circuits, by replacing all the J gates with a small CME pattern, we could move all the entanglement to the beginning of the circuit and all the corrections to the final part, given the measurement calculus [26]. We obtain a practical MQC plan where qubits are connected in the graph representing CZ gates, and measurements are performed sequentially, adapting the measurement basis based on previous outcomes. Overall the CME pattern could be summarized as:

$$U := [C][M][E]. \quad (1)$$

Invested Magic Resources and Upper Bound for Quantum Fourier Transform (QFT) — From a resource-theoretic perspective, introducing auxiliary qubits in the $|+\rangle$ state, entangling them with CZ gates, and applying final Pauli corrections do not require any magic resources. As such, during the whole MQC procedure, the key source of magic resource investment lies in the non-Pauli measurements. These measurements lead to the generation of states with higher magic content, which is ultimately reflected in the final output state of the computation.

The randomness in the outcomes $\{s_i\}$ is crucial for MQC, however, it has no effect from the point of view of magic resources. The final projected state of each adaptive measurements is $\frac{1}{\sqrt{2}}(|0\rangle + (-1)^{s_o} e^{is_i\theta}|1\rangle)$, depending on the values of previous measurement outcomes (s_i) and this measurement outcome (s_o). Indeed, the Pauli spectrum $\Xi_P := d^{-1}\langle\psi|P|\psi\rangle^2$ of these states remains the same regardless of the stochastic measurement outcomes and uses the stabilizer α -Renyi entropy (SRE) as magic measure of the output state [7], $\mathbb{M}_\alpha(|\psi\rangle) := (1 - \alpha)^{-1} \log \sum_P \Xi_P^\alpha - \log d$. Therefore the magic resources required for a single qubit measurement $\mathbb{M}_\alpha(\theta) = \mathbb{M}_\alpha((|0\rangle + e^{i\theta}|1\rangle)/\sqrt{2})$, are independent of the

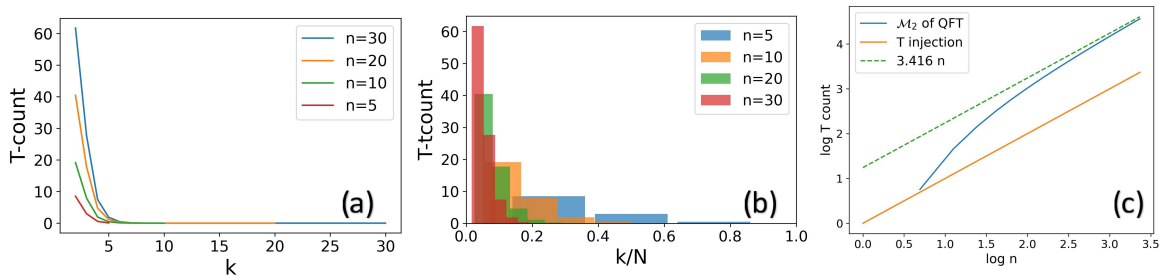


FIG. 2. *Demonstration of invested magic resources in QFT.* (a) and (b) show the distribution of invested magic resources across different frequencies k , with a concentration of resources in the lower-frequency range. (c) illustrates the scaling of invested magic resources with the number of qubits, with the 'T injection' curve representing MSI with T-counts equal to n . This provides a direct comparison between the two methods for generating magic states.

signal values. Specifically, for the 2-Rényi entropy, we have $\mathbb{M}_2(\theta) = -\log(\frac{1}{2}\cos^4\theta + \frac{1}{2}\sin^4\theta + \frac{1}{2})$. By additivity of the SRE, a n -qubit $\otimes J(\theta)$ requires $n\mathbb{M}_2(\theta)$ magic resources.

The single-qubit state containing maximum magic resources is Kitaev's T-state [5], $|T\rangle = \cos\theta_m|0\rangle + \sin\theta_m e^{i\pi/4}|1\rangle$ with $\cos 2\theta_m = 1/\sqrt{3}$. In the later discussion, we use the one T-state magic resource $1T = \mathbb{M}_2(|T\rangle)$ as a unit to scale magic resources, denoted as *T-count*.

Since each measurement setting in MQC corresponds to a J gate with angle θ in the J-decomposition of the target unitary U in Eq.(1), we can define the total *invested magic resources* for implementing U as:

$$\mathcal{M}_\alpha(U) := \sum_{J(\theta)} \mathbb{M}_\alpha(\theta). \quad (2)$$

For example, the arbitrary rotation on the single qubits, $U = J(0)J(\alpha)J(\beta)J(\gamma)$. The corresponding magic resources on MQC is $\mathcal{M}_\alpha(U) = \mathbb{M}_\alpha(\alpha) + \mathbb{M}_\alpha(\beta) + \mathbb{M}_\alpha(\gamma)$. From the Eq. (2), the magic measure for unitary operations is *gate-order-independent*, thanks to the measurement calculus rule. Gate-order independence refers to the fact that the total invested magic resources remain unchanged regardless of the order in which quantum gates are applied. This simplifies the framework for quantifying computational costs in quantum circuits.

This invested magic resource \mathcal{M}_α possesses the essential properties of a *good* magic resource measure. It exhibits faithfulness, meaning $\mathcal{M}_\alpha(C) = 0$ if and only if C is a Clifford gate. Additionally, \mathcal{M}_α is invariant under Clifford gates, meaning $\mathcal{M}_\alpha(CU) = \mathcal{M}_\alpha(U)$ for any Clifford gate C , as applying C before or after U does not change the magic resource cost. Finally, \mathcal{M}_α satisfies additivity, meaning $\mathcal{M}_\alpha(U \otimes V) = \mathcal{M}_\alpha(U) + \mathcal{M}_\alpha(V)$. The proof is left in Sec. III in [27].

The invested magic resource measure \mathcal{M}_α offers a unique perspective compared to previous magic resource quantifiers. First, \mathcal{M}_α is naturally defined at the process level. Moreover, it is directly derived from the magic

content of single-qubit states. Most importantly, while previous measures typically provide lower bounds on the magic resources required for a given task, \mathcal{M}_α serves to quantify a sufficient amount of resources for the task and also as a *witness* of employed magic resources. This means that if a quantum computation has an invested magic resource cost of \mathcal{M}_α , there exists a concrete MQC implementation using that amount of magic resources.

The invested magic resource framework provides a useful tool for analyzing the complexity of quantum Fourier transformation (QFT), offering an upper bound on the resources required for its implementation. QFT is a circuit which maps position basis $|x\rangle$ into frequency basis $|k\rangle$ with many Hadamard gates and controlled-rotation gates (CR_k) with $R_k = \text{diag}[1, \exp(i2\pi/2^k)]$. Given the J-decomposition of the controlled-rotation gates, we have:

$$\begin{aligned} \mathcal{M}_2(\text{QFT}) &= \sum_{k=2}^n (n+k-1)\mathcal{M}_2(CR_k) \\ &\approx 3.4619n - 5.3388. \end{aligned} \quad (3)$$

as demonstrated in Fig. 2 (c). See Sec. IV of [27] for the derivation.

Fig. 2 (a) and (b) visualize the contribution of different frequencies to the invested magic resources of QFT. The plots reveal that most of the magic resources are concentrated in the low-frequency range, with a sharp decline in contribution as the frequency increases. This behavior remains consistent across different qubit numbers. Previous analyses of classical simulation algorithms for QFT circuits have suggested a complexity of $O(n \log n)$ T gates [28]. However, the invested magic resource framework provides an upper bound on the required resources, indicating that $O(n)$ T gates are sufficient.

Potential Magic resources— While designing specific graphs for targeted tasks is one approach to MQC, a more general strategy involves preparing versatile graph states capable of performing arbitrary quantum computations. These versatile graphs are often referred to as universal resources for MQC [22–24]. However, it is important to recognize that not all invested magic resources effectively

contribute to the magic content of the final state. This limitation arises from the inherent maximum potential of magic resources that a particular graph type can hold.

We define reserved magic resources \mathcal{R} and potential magic resources \mathcal{P} in the following way. Given a preparation obtained by a set of single-qubit measurements $[M]$ (obeying MQC law) on a graph state $|G\rangle$, its reserved and potential magic resource are defined as

$$\mathcal{R}([M]|G) := \mathbb{M}_2([M]|G), \quad \mathcal{P}(|G) := \max_{[M]} \mathcal{R}([M]|G). \quad (4)$$

The above definition is motivated by the fact that the entanglement structure is fundamental to determine how much magic can be hosted in a certain state, compared to the simple additive structure in factorized states [29]. Additionally, MQC allows for a general quantum input. Given an input state $|\psi\rangle \in \mathcal{H}_{in}$ the graph state can be seen as the Choi isomorphic state of the channel $G : \mathcal{H}_{in} \rightarrow \mathcal{H}_{out}$ as $|G\rangle \in \mathcal{H}_{in} \otimes \mathcal{H}_{out}$. Then, we have $[E]|\psi\rangle = |G\rangle * |\psi\rangle \in \mathcal{H}_{out}$, with $*$ as link product [30, 31] between the graph and the input state and $|G\rangle$ as a graph with some links vacant. The maximum increment of potential magic resources brought by the entanglement structure with the input $|\psi\rangle$ is thus $\mathcal{P}(G; |\psi\rangle) := \max_{[M]} \mathbb{M}_2([M]|G * |\psi\rangle) - \mathbb{M}_2(|\psi\rangle)$.

Therefore, if MQC can produce a state $|\phi\rangle$ or its Clifford equivalents from the input state $|\psi\rangle$ with a graph $|G\rangle$, denoted as $|G\rangle * |\psi\rangle \geq_{\text{MQC}} |\phi\rangle$, the potential magic resources must satisfy $\mathcal{P}(|G; |\psi\rangle) \geq \mathbb{M}_2(|\phi\rangle) - \mathbb{M}_2(|\psi\rangle)$. Consequently, a family of graph states can serve as universal resources only if their potential magic resources scale as n^α , where $\alpha > 0$ and n is the number of qubits.

A key application of this concept lies in demonstrating the limitations of linear graphs and GHZ states as universal resources, regardless of their size. From the perspective of potential magic resources, we can show that:

$$\mathcal{P}(|\text{Linear}\rangle) = 1T, \quad \mathcal{P}(|\text{GHZ}\rangle) = 1T. \quad (5)$$

For a definition of the linear graph states $|\text{Linear}\rangle$ and a proof see Sec. V in [27].

The fact that linear and GHZ states have limited potential magic resources implies that the computational power they offer through magic resources is constant and does not scale with the system size. This finding provides a novel perspective on the concept of universality in MQC, highlighting the importance of potential magic resources as a measure of the capability of different graph structures.

Potential magic resources constrain the computational power of MQC for different graph types. However, detailed calculations can be challenging. Therefore, we provide a general bound for the potential magic resources by considering d-dimensional graphs as

$$\mathcal{P}(|G\rangle)_{\min} = O(n^{(d-1)/d}) \quad (6)$$

For $d=1$, $\mathcal{P}(|G\rangle)_{\min} \sim \text{const}$, we observe a constant gap between MQC and classical simulation, as seen in the linear graph. For 2-D graph, $\mathcal{P}(|G\rangle)_{\min} \sim \sqrt{n}$, we get a super-linear gap, for $\sqrt{n} \geq \log n$ when n is large. Finally, as a high-dimensional graph, we have $\mathcal{P}(|G\rangle)_{\min} \rightarrow n$, which leads to an exponential gap between MQC and classical computation. For details of this part, see Sec. VI in [27].

The relationship between the invested magic resources (\mathcal{M}), potential magic resources (\mathcal{P}), and reserved magic resources (\mathcal{R}) are summarized in Fig. 1 using the analogy of pouring water into a glass. While invested magic resources represent the total resources required during the computation process, potential magic resources reflect the maximum achievable magic resources that a given graph structure can support. The gap between these two measures provides insights into the efficiency of the quantum computation. And any excess water that spills over signifies wasted magic resources, which could be defined as $\mathcal{W} = \mathcal{M} - \mathcal{P}$.

Experimental Results — The invested magic resources, \mathcal{M}_2 , enable us to quantify the magic resources injected into the network in MQC. The magic resources of the remaining state after each step of measurement, \mathcal{R} , represent the reserved magic resources. By introducing these concepts, we can indicate the invested and reserved magic resources step by step in the MQC process.

We focus on two typical processes: single-qubit rotation and QFT. We demonstrate how the magic responds to single-qubit measurements in 1-D and 2-D graph states. The 1D graph state is a linear state, while the 2D graph state is a BOX state. Both originate from the 4-qubits cluster state, $|\text{cluster}\rangle = (|0000\rangle + |0011\rangle + |1100\rangle - |1111\rangle)/2$ [32]. For the specific setup see Sec. VII in [27]. The experimental estimation of reserved magic resources derives from the few-shot randomized measurements [33, 34], see Sec. VIII in [27].

Our experiment utilizes a linear graph and MQC to generate the $|T\rangle$ state. The process can be mathematically expressed with a cluster state in the CME pattern as:

$$|T\rangle = X^{s_2} Z^{s_1+s_3} [M_3^{\pi/4}]^{s_2} [M_2^{\theta_m}]^{s_1} [M_1^0] |\text{cluster}\rangle. \quad (7)$$

Here, s_i represents the binary measurement outcome on the i th measurement. Although the measurement outcomes on each qubit are random and influence subsequent measurement settings and corrections, our previous analysis established that they do not affect the overall magic resources within the system. Therefore, we average the final magic resources over all possible single-qubit measurement outcomes to obtain an estimation.

The comparison between the invested and reserved magic resources in the process is illustrated in Fig. 3(a). The reserved magic resources are 0, 0.62T, and 1T, with accumulated invested magic resources of 0T, 0.62T, and 1.33T, respectively. It can be seen that the invested and

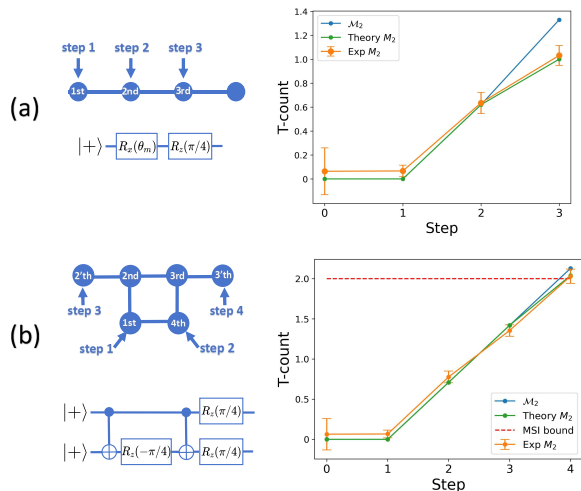


FIG. 3. (a) Experimental generation of the $|T\rangle$ state using a 1D graph in three steps. The angles of M^θ are $0, \theta_m, \pi/4$ for steps 1, 2, and 3, respectively. The plot on the right displays the total invested magic resources \mathcal{M}_2 and the reserved magic resource \mathcal{R} at each step. (b) Experimental realization of QFT using a 2D graph. The left side of the figure depicts the 2D graph structure employed for implementing the QFT circuit of $n = 2$ (left bottom) and indicates the order of measurements performed on the qubits (steps 1 to 4). The generation of $|\text{CS}\rangle$ from MQC requires at least 6 qubits, as the figure shows. Step 3 on the 2'th qubit and step 4 on the 3'th qubit are equivalent to the local rotation for the physical qubits 2nd and 3rd qubit. According to Eq.(8), implementing $M_1^0, M_4^{(\pi/8,0)}, \hat{T}_2$, and \hat{T}_3 corresponds to the steps 1 to 4, in which $M_4^{(\pi/8,0)}$ is for non-standard measurement $M^{(\phi,\theta)}$, projection onto $\{\cos\phi|0\rangle \pm e^{-i\theta}\sin\phi|1\rangle\}$, and \hat{T} is T-gate $\hat{T} = \text{diag}[1, e^{i\pi/4}]$. Move experimental results see Sec. IX and Sec. X in [27].

reserved magic are equal during the first two steps of the process. However, for the third step, a waste of magic resources $\mathcal{W} = 0.33T$ is inevitable because the invested magic resources exceed the potential magic resources for a linear graph $\mathcal{P} = 1T$.

We demonstrate the generation of QFT of $n = 2$ in MQC. QFT requires controlled-rotation gates with arbitrary angles. Here for $n = 2$, it shows $CR_2 = \text{diag}[1, 1, 1, i]$, also known as CS gate. The power of QFT is evident in the resulting QFT state, defined as $|\text{QFT}_n\rangle = \text{QFT}_n|+\rangle|0\rangle^{\otimes(n-1)}$, which possesses a nullity of $\nu(|\text{QFT}_n\rangle) = n - 2$ [18]. For $n = 2$, the QFT state $|\text{QFT}_2\rangle = |\text{CS}\rangle = (|00\rangle + |01\rangle + |10\rangle + i|11\rangle)/2$, representing the state with maximum magic content for a two-qubit system, can be generated from the MQC, see Fig. 3(b). The resulting CME pattern for generating the $|\text{CS}\rangle$ state is given by:

$$|\text{CS}\rangle = X_3 Z_3^4 Z_2^{s_1} \hat{T}_3 \hat{T}_2 [M_4^{(\pi/8,0)}][M_1^0]|\text{cluster}\rangle. \quad (8)$$

The invested magic resources increase by approximately $0.71T$ with each step of the process. Conse-

quently, the accumulated invested magic resources for steps 1 to 4 are $0T, 0.71T, 1.42T$, and $2.13T$, respectively. The corresponding reserved magic resources are $0T, 0.71T, 1.41T$, and $2.03T$. The inevitable wasted magic resources are merely $\mathcal{W} = 0.1T$. In the experiments, we obtain $0.066 \pm 0.024T, 0.777 \pm 0.036T, 1.354 \pm 0.036T, 2.030 \pm 0.045T$. Notably, almost all the invested magic resources are effectively injected into the system until the potential $\mathcal{P} = 2.03T$, bringing the inevitable waste of $\mathcal{W} = 0.1T$.

Furthermore, MQC offers a significant advantage over the conventional MSI approach. With MSI, the maximum achievable magic resources for an n -qubit state are limited to nT . However, MQC, by strategically employing auxiliary qubits and sequential measurements, can generate states with magic content exceeding the qubit number. For example, the $|\text{CS}\rangle$ state, while comprising only 2 qubits, contains $2.03T$ of magic, and the Hoggar state, a 3-qubit state, holds $3.6T$ of magic. Both of these states can be efficiently generated using MQC, demonstrating its space-saving potential for quantum processors. More discussions in Sec. XI of [27].

Discussion — This work introduces two key concepts, *invested* and *potential* magic resources, providing new insights into the role of magic in MQC, especially the role of non-Pauli measurements. Moreover, our work also offers a fresh perspective on the universality of MQC from magic, where we show that high-dimensional graph states can induce a superlinear—or even exponential—advantage over classical computation. Experimental results further validate our theoretical predictions, revealing that the reserved magic resources would increase with each non-Pauli measurement step.

Our framework establishes MQC as a promising approach for magic state generation and utilization, particularly in resource-efficient implementations of quantum algorithms such as QFT. Future research could focus on optimizing MQC for large-scale quantum networks, paving the way for more robust and fault-tolerant quantum computation.

Acknowledgement — This work was supported by the Innovation Program for Quantum Science and Technology (Nos. 2021ZD0301200, 2021ZD0301400, 2021ZD0302000), National Natural Science Foundation of China (Grant Nos. 12350006, 12205048, 11821404), Anhui Initiative in Quantum Information Technologies (AHY060300), Shanghai Science and Technology Innovation Action Plan (Grant No. 24LZ1400200), USTC Research Funds of the Double First-Class Initiative (Grant No. YD2030002026). AH acknowledges support from PNR MUR project PE0000023-NQSTI and PNR MUR project CN 00000013 -ICSC.

* you_zhou@fudan.edu.cn

† chengeng@ustc.edu.cn

‡ cfi@ustc.edu.cn

§ alioscia.hamma@unina.it

- [1] E. T. Campbell, B. M. Terhal, and C. Vuillot, Roads towards fault-tolerant universal quantum computation, *Nature* **549**, 172 (2017).
- [2] L. Postler, S. Heußen, I. Pogorelov, M. Rispler, T. Feldker, M. Meth, C. D. Marciniak, R. Stricker, M. Ringbauer, R. Blatt, *et al.*, Demonstration of fault-tolerant universal quantum gate operations, *Nature* **605**, 675 (2022).
- [3] G. Q. AI, Suppressing quantum errors by scaling a surface code logical qubit, *Nature* **614**, 676 (2023).
- [4] R. S. Gupta, N. Sundaresan, T. Alexander, C. J. Wood, S. T. Merkel, M. B. Healy, M. Hillenbrand, T. Jochym-O'Connor, J. R. Wootton, T. J. Yoder, *et al.*, Encoding a magic state with beyond break-even fidelity, *Nature* **625**, 259 (2024).
- [5] S. Bravyi and A. Kitaev, Universal quantum computation with ideal clifford gates and noisy ancillas, *Phys. Rev. A* **71**, 022316 (2005).
- [6] V. Veitch, S. H. Mousavian, D. Gottesman, and J. Emerson, The resource theory of stabilizer quantum computation, *New Journal of Physics* **16**, 013009 (2014).
- [7] L. Leone, S. F. Oliviero, and A. Hamma, Stabilizer rényi entropy, *Phys. Rev. Lett.* **128**, 050402 (2022).
- [8] L. Leone and L. Bittel, Stabilizer entropies are monotones for magic-state resource theory, *Phys. Rev. A* **110**, L040403 (2024).
- [9] A. M. Souza, J. Zhang, C. A. Ryan, and R. Laflamme, Experimental magic state distillation for fault-tolerant quantum computing, *Nature communications* **2**, 169 (2011).
- [10] E. Knill, Quantum computing with realistically noisy devices, *Nature* **434**, 39 (2005).
- [11] M. Howard and E. Campbell, Application of a resource theory for magic states to fault-tolerant quantum computing, *Phys. Rev. Lett.* **118**, 090501 (2017).
- [12] B. Regula and R. Takagi, Fundamental limitations on distillation of quantum channel resources, *Nature Communications* **12**, 4411 (2021).
- [13] S. Aaronson and D. Gottesman, Improved simulation of stabilizer circuits, *Phys. Rev. A* **70**, 052328 (2004).
- [14] S. Bravyi and D. Gosset, Improved classical simulation of quantum circuits dominated by clifford gates, *Phys. Rev. Lett.* **116**, 250501 (2016).
- [15] S. Bravyi, G. Smith, and J. A. Smolin, Trading classical and quantum computational resources, *Phys. Rev. X* **6**, 021043 (2016).
- [16] V. Veitch, S. H. Mousavian, D. Gottesman, and J. Emerson, The resource theory of stabilizer quantum computation, *New Journal of Physics* **16**, 013009 (2014).
- [17] X. Wang, M. M. Wilde, and Y. Su, Efficiently computable bounds for magic state distillation, *Phys. Rev. Lett.* **124**, 090505 (2020).
- [18] M. Beverland, E. Campbell, M. Howard, and V. Kliuchnikov, Lower bounds on the non-clifford resources for quantum computations, *Quantum Science and Technology* **5**, 035009 (2020).
- [19] O. Hahn, A. Ferraro, L. Hultquist, G. Ferrini, and L. García-Álvarez, Quantifying qubit magic resource with Gottesman-Kitaev-Preskill encoding, *Phys. Rev. Lett.* **128**, 210502 (2022).
- [20] S. F. Oliviero, L. Leone, and A. Hamma, Transitions in entanglement complexity in random quantum circuits by measurements, *Phys. Lett. A* **418**, 127721 (2021).
- [21] P. Niroula, C. D. White, Q. Wang, S. Johri, D. Zhu, C. Monroe, C. Noel, and M. J. Gullans, Phase transition in magic with random quantum circuits, *Nature physics* **20**, 1786 (2024).
- [22] H. J. Briegel, D. E. Browne, W. Dür, R. Raussendorf, and M. Van den Nest, Measurement-based quantum computation, *Nature Physics* **5**, 19 (2009).
- [23] M. Van den Nest, W. Dür, A. Miyake, and H. J. Briegel, Fundamentals of universality in one-way quantum computation, *New Journal of Physics* **9**, 204 (2007).
- [24] M. Van den Nest, A. Miyake, W. Dür, and H. J. Briegel, Universal resources for measurement-based quantum computation, *Phys. Rev. Lett.* **97**, 150504 (2006).
- [25] V. Danos, E. Kashefi, and P. Panangaden, Parsimonious and robust realizations of unitary maps in the one-way model, *Phys. Rev. A* **72**, 064301 (2005).
- [26] V. Danos, E. Kashefi, and P. Panangaden, The measurement calculus, *Journal of the ACM (JACM)* **54**, 8 (2007).
- [27] Supplementary material.
- [28] Y. Nam, Y. Su, and D. Maslov, Approximate quantum fourier transform with $o(n \log(n))$ gates, *NPJ Quantum Information* **6**, 26 (2020).
- [29] D. Iannotti, G. Esposito, L. C. Venuti, and A. Hamma, Entanglement and stabilizer entropies of random bipartite pure quantum states (2025), [arXiv:2501.19261 \[quant-ph\]](https://arxiv.org/abs/2501.19261).
- [30] G. Chiribella, G. M. D'Ariano, and P. Perinotti, Quantum circuit architecture, *Phys. Rev. Lett.* **101**, 060401 (2008).
- [31] G. Chiribella, G. M. D'Ariano, and P. Perinotti, Theoretical framework for quantum networks, *Phys. Rev. A* **80**, 022339 (2009).
- [32] P. Walther, K. J. Resch, T. Rudolph, E. Schenck, H. Weinfurter, V. Vedral, M. Aspelmeyer, and A. Zeilinger, Experimental one-way quantum computing, *Nature* **434**, 169 (2005).
- [33] Y. Zhou, P. Zeng, and Z. Liu, Single-copies estimation of entanglement negativity, *Phys. Rev. Lett.* **125**, 200502 (2020).
- [34] G.-C. Li, L. Chen, S.-Q. Zhang, X.-S. Hong, Y. Zhou, G. Chen, C.-F. Li, and G.-C. Guo, Directly estimating mixed-state entanglement with bell measurement assistance, [arXiv preprint arXiv:2405.20696](https://arxiv.org/abs/2405.20696) (2024).